

FACULTY OF SCIENCE
PALACKÝ UNIVERSITY OLOMOUC

Department of Optics



**Tunable filters and variable interaction
using polarization interferometers
and liquid crystals**

DIPLOMA THESIS

Vojtěch Krčmarský

2016

FACULTY OF SCIENCE
PALACKÝ UNIVERSITY OLOMOUC

Department of Optics



**Tunable filters and variable interaction
using polarization interferometers
and liquid crystals**

DIPLOMA THESIS

Author:

Bc. Vojtěch Krčmarský

Study program:

N1701 Physics

Field of study:

Optics and Optoelectronics

Supervisor:

Mgr. Miroslav Ježek, Ph.D.

PŘÍRODOVĚDECKÁ FAKULTA
UNIVERZITY PALACKÉHO V OLOMOUCI

Katedra optiky



**Laditelná filtrace a interakce
v polarizačních interferometrech
s tekutými krystaly**

DIPLOMOVÁ PRÁCE

Vypracoval:

Bc. Vojtěch Krčmarský

Studijní program:

N1701 Fyzika

Studijní obor:

Optika a optoelektronika

Vedoucí diplomové práce:

Mgr. Miroslav Ježek, Ph.D.

Abstract

Polarization state control plays a crucial role in many quantum optics and quantum information experiments, where information is coded into polarization degree of freedom of light. The manipulation with polarization state and its measurement are inevitable parts of every such experiment. Standard methods for manipulation with polarization require physical movement of quarter wave plates and half wave plates. This movement takes time proportional to an angle of rotation and brings some other issues.

The liquid crystal technology is a one of alternatives to increase the speed of polarization changes during experiments. The advantages of this approach are the absence of moving parts and fast polarization changes induced by changing the voltage applied to the devices.

In this Thesis, liquid crystal modules, based on simple liquid crystal displays are characterized and used to perform fast polarization measurements using minimal tomography, phase modulation in the Mach-Zehnder interferometer, and polarization filtering.

Results, presented in this Thesis, show that liquid crystal modules, made of common liquid crystal displays can be used in many quantum optics experiments, including experiments with interferometers.

Key words

polarization, liquid crystal, liquid crystal module, polarization state analysis, polarimetry, minimal quantum state tomography, phase modulator, polarization filter

Acknowledgements

I am deeply grateful to my supervisor Mgr. Miroslav Ježek. Without his guidance and persistent help, this thesis would not have been possible. I am grateful to all colleagues, namely Martina Miková, Ivo Straka, Josef Hloušek, Jan Bílek, Jaromír Běhal, and Robert Stárek, for their friendly attitude and creating supporting and creative environment. I owe my deepest gratitude to my family for their love, support, patience and understanding during these years. Last, but not least, I would like to thank my roommates Pavel Zoufalý and Marek Machata for cheering up.

Declaration

I declare that I have written Diploma Thesis “Tunable Filters and variable interaction using polarization interferometers and liquid crystals” on my own under the guidance of Mgr. Miroslav Ježek, Ph.D. by using theoretical resources, which are referred to in the list of literature. I agree with the further usage of this document according to the requirements of the Department of Optics.

In Olomouc on

.....
Vojtěch Krčmarský

Contents

Introduction	1
1 Polarization of light	3
1.1 Describing polarization	3
1.2 Transformation of polarization	5
1.3 Polarization state tomography	6
1.4 Quantum process tomography	7
2 Nematic liquid crystal technology	9
2.1 TN LC devices	10
2.2 LC device drivers	10
2.3 Used LC modules	12
3 Theoretical model	14
4 Single module characterization	15
5 Polarization state preparation and analysis using LC modules	17
5.1 Minimal quantum state tomography	17
5.2 Wave plate preparation and analysis	18
5.3 LC PA unit 1	19
5.4 LC PA unit 2	21
5.5 The response of polarization preparation and analysis	24
6 Polarization filter	29
6.1 Polarization interferometer	29
6.2 Polarization filter with one LC module	30
7 Tunable phase modulator	33
8 Polarization filter with phase modulator	35
Conclusion	38
References	40

Introduction

Quantum information processing became the merit of interest for its broad applications in secure communication, quantum metrology or quantum lithography [1]. Quantum information experiments could be performed on many platforms. Advanced experiments were performed with trapped ions [2], atoms, nuclear magnetic resonance, superconducting quantum circuits [3], and photons [4].

The quest of quantum information processing is to develop a quantum computer that provides us with ultrafast factoring and potential to perform simulations of quantum system dynamics [4]. The main requirements for the universal quantum computer were proposed by *DiVincenzo* in [5]. Quantum computing with photons satisfies most of these criteria. Photons, as information carriers, interact with the surrounding environment weakly, but can be easily manipulated to create a quantum bit. In 2001 *E. Knill, R. Laflamme and G. J. Milburn* showed that linear optics is sufficient for quantum information processes with photons [6]. This discovery opened great interest in the quantum optics experiments.

Properties of photons enable performing communication tasks, such as long distance quantum teleportation, where current record distance is more than 100 km in optical fibre [7] and even in free space [8]. This was also used in the recent tests of Bell inequality [9].

Another large group of quantum information experiments deals with the construction of quantum logic gates. These gates use different degrees of freedom of the photon such as polarization, time-bin or path to encode the information [1, 4]. At the output of these experiments, the information has to be read out. For quantum bits encoded in polarization, it means to perform polarimetric measurements. The number of measurements increases exponentially with a number of qubits processed in the experiment. This is a reason why developing faster polarization measurements is of high importance.

A possible approach to speed up measurements is to use liquid crystals. These were used in experiments as variable phase retarders, simulating rotational wave plate with voltage dependent retardation [10], polarization rotators [11], or polarization controllers [12, 13]. These devices were used in quantum optics experiments, creating for example depolarization channels [14], or in quantum cryptography protocols [15]. The fast polarization changes are desirable for creating optical shutters [16] and switches [17]. These devices find use in quantum memory experiments, quantum logic gates, and quantum key

distribution.

The liquid crystal technology can find great application in quantum random walks on a photonic platform. A quantum random walk is an alternative approach for quantum computing and simulations [18, 19]. These experiments are based on multiple path interferometers, where each path has to be addressed individually [20]. This is difficult to perform with standard elements, such as quarter and half wave plates. On the other hand, custom design of liquid crystal module could make this task easy.

Liquid crystals find application in many other branches of optical experiments. They are, for example, broadly used in spatial light modulators. These devices are used to transform a wavefront of a light wave and create various vortex beams [21]. Another application can be found in digital holography [22]. The polarization properties of such device were analysed at our department by *J. Běhal* [23].

The aim of this Thesis is to show the possible application of the liquid crystal technology for quantum information processing and polarimetry. Three types of devices - units for polarization state preparation and analysis, polarization filters, and phase modulator - will be presented in this Thesis. The liquid crystal modules were made of liquid crystal displays available in almost any shop with electronic components. These devices can be directly used in quantum optics experiments.

1 Polarization of light

Let us consider a monochromatic plane wave with frequency ν and corresponding angular frequency $\omega = 2\pi\nu$ propagating in a direction of z axis with velocity c . The electric field is described by following equation:

$$\mathcal{E}(z, t) = \text{Re} \left\{ \mathbf{A} \exp \left[i\omega \left(t - \frac{z}{c} \right) \right] \right\}, \quad (1)$$

where $\mathbf{A} = A_x \hat{\mathbf{x}} + A_y \hat{\mathbf{y}}$ is a vector with complex components A_x and A_y [24]. To describe the polarization of this wave, we have to trace the endpoint of the vector $\mathcal{E}(z, t)$. The following equation describes generic polarization ellipse [24, 25]:

$$\frac{\mathcal{E}_x^2}{a_x^2} + \frac{\mathcal{E}_y^2}{a_y^2} - 2 \frac{\mathcal{E}_x \mathcal{E}_y}{a_x a_y} \cos \varphi = \sin^2 \varphi, \quad (2)$$

where \mathcal{E}_x and \mathcal{E}_y are x and y components of the electric field with amplitudes a_x and a_y respectively and $\varphi = \varphi_y - \varphi_x$ is a phase difference between \mathcal{E}_x and \mathcal{E}_y .

The orientation and shape of this ellipse, given by the phase difference φ and balance of amplitudes a_x and a_y , determine the polarization state of light. We talk about right-handed elliptical polarization in case of rotation clockwise and in case of counter clockwise rotation, we talk about left-handed elliptical polarization. In special cases, when $\varphi = 0$ or π , the polarization ellipse collapses into line and we talk about linear polarization. If phase difference $\varphi = \frac{\pi}{2}$ and $a_x = a_y$, the ellipse becomes a circle and we talk about right circular polarization. For $\varphi = -\frac{\pi}{2}$ and $a_x = a_y$, we talk about left circular polarization.

1.1 Describing polarization

Jones vectors

Let us consider a plane monochromatic wave with frequency ν propagating along the z axis. This wave is fully characterized by the complex envelopes $A_x = a_x \exp(i\varphi_x)$ and $A_y = a_y \exp(i\varphi_y)$ of the x and y components of the vector of electric field. These complex amplitudes can be written as a column vector - Jones vector \mathbf{J} [26],

$$\mathbf{J} = \frac{1}{\sqrt{A_x^2 + A_y^2}} \begin{pmatrix} A_x \\ A_y \end{pmatrix}. \quad (3)$$

Jones vectors are normalized such that $\|\mathbf{J}\| = \mathbf{J}^\dagger \mathbf{J} = 1$, where \dagger denotes Hermitian conjugation, and describe only pure polarization states [25].

For single photons, the Jones vectors can be interpreted, in analogy with two level quantum system, as a description of a pure quantum state $J \equiv |J\rangle$.

Stokes vectors

Every polarization state can be represented as a point in a 3D configuration space. Each point can be defined in Cartesian coordinates with three independent coordinates S_1 , S_2 , and S_3 , or in spherical coordinates with two angles χ and ψ and the distance from the origin of the coordinate system S_0 . Cartesian coordinates can be determined from spherical as:

$$S_1 = S_0 \cos 2\chi \cos 2\psi, \quad (4a)$$

$$S_2 = S_0 \cos 2\chi \sin 2\psi, \quad (4b)$$

$$S_3 = S_0 \sin 2\chi. \quad (4c)$$

From Eqs. (4a-c) it is obvious that following is satisfied:

$$S_0^2 = S_1^2 + S_2^2 + S_3^2. \quad (5)$$

The parameters S_0 , S_1 , S_2 , and S_3 are called Stokes parameters. The parameter S_0 goes from 0 for completely unpolarized light to 1 for pure polarization states and its value defines the degree of polarization (DOP). Therefore, every polarization state can be geometrically represented on a sphere - Poincare sphere. Pure states lie on the surface of the sphere, while mixed states are inside the sphere [24]. The Poincare sphere is depicted in Fig. 1.

Density matrix

This approach allows us to describe either pure states and mixed states equally. The density matrix is a 2×2 Hermitian matrix with $\text{Tr}[\rho] = 1$. In analogy with the two level mixed quantum system, the polarization state can be represented as

$$\rho = \sum_k p_k |k\rangle \langle k|, \quad (6)$$

where p_k is the probability of finding the pure state $|k\rangle$ (Jones vector) in the given mixture ρ . The density matrix is connected with Stokes parameters,

$$\rho = \frac{1}{2} \left(\sigma_0 + \sum_{i=1}^3 S_i \sigma_i \right). \quad (7)$$

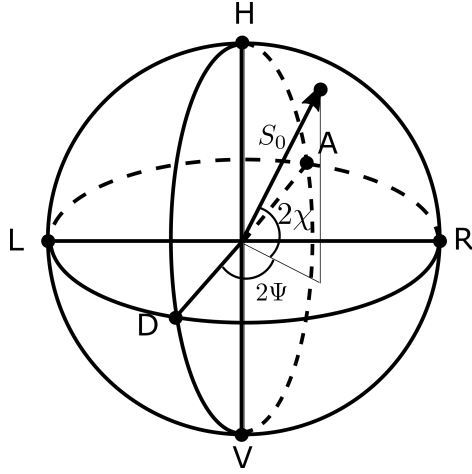


Figure 1: Poincaré sphere.

Here S_i are Stokes parameters and σ_i are corresponding Pauli matrices:

$$\sigma_1 = \begin{pmatrix} 0 & 1 \\ 1 & 0 \end{pmatrix}; \sigma_2 = \begin{pmatrix} 0 & -i \\ i & 0 \end{pmatrix}; \sigma_3 = \begin{pmatrix} 1 & 0 \\ 0 & -1 \end{pmatrix}; \sigma_0 = \begin{pmatrix} 1 & 0 \\ 0 & 1 \end{pmatrix}. \quad (8)$$

1.2 Transformation of polarization

Polarization of light wave could be transformed by many types of optical elements. The most common elements are based on birefringence or selective absorption. It is of high importance to describe the effect of such elements on the electric field of light, especially on its polarization.

Fully polarized light described by Jones vector \mathbf{J} is transformed by 2×2 matrix called Jones matrix. In analogy with a quantum information, the transformation of polarization could be treated as transformation of any other qubit. The output polarization \mathbf{J}_{out} after propagating through a system described by Jones matrix T is determined as follows.

$$\mathbf{J}_{\text{out}} = T \cdot \mathbf{J}_{\text{in}}, \quad (9)$$

where \mathbf{J}_{in} is Jones vector of input polarization state. The matrix of a system T usually consists of multiple polarization elements. The matrix of the whole system is determined by matrix multiplying of elements in opposite order to their organisation in the experiment. For example, If light propagates first through element described by Jones matrix T_1 followed by element with Jones matrix T_2 , then the matrix of the whole system will be

$T = T_2 \cdot T_1$. The mixed states are transformed as $\rho_{\text{out}} = T \cdot \rho_{\text{in}} \cdot T^\dagger$

The basic operations on quantum bits are based on Pauli matrices, presented in Eq. (8). A continuous family of single-qubit rotations could be achieved when Pauli matrices are exponentiated. Any unitary transformation could be achieved by combining these matrices [27].

Following matrices define principal polarization transformations:

$$P = \begin{pmatrix} 1 & 0 \\ 0 & 0 \end{pmatrix}; R(\vartheta) = \begin{pmatrix} \cos \vartheta & \sin \vartheta \\ -\sin \vartheta & \cos \vartheta \end{pmatrix}; T(\Gamma) = \begin{pmatrix} 1 & 0 \\ 0 & \exp\{-i\Gamma\} \end{pmatrix}. \quad (10)$$

Here P is a Jones matrix of linear polariser oriented along the x axis, $R(\vartheta)$ is matrix of rotation of angle ϑ and $T(\Gamma)$ is matrix of phase retarder with retardation Γ with optical axis parallel with the x axis.

1.3 Polarization state tomography

The goal of the polarization state tomography is to determine polarization state of light represented by its density matrix from measured data. The unknown polarization state can not be determined using only one measurement, but a large ensemble of photons is required for the procedure. These photons are projected onto multiple different polarization states.

Four measurements are required for successful polarization state reconstruction. Three measurements are needed to find parameters of the polarization state and the fourth to determine normalisation [28, 29].

We can use direct reconstruction procedure to estimate elements of the density matrix. This method uses measured data as mean values of density matrix in respect to given base state Ψ_i . These represent probability of finding state in given projection

$$p_i = \langle \Psi_i | \rho | \Psi_i \rangle. \quad (11)$$

The elements of density matrix ρ can be found by reverting the Eq. (11) [29]. This procedure is feasible and easy to implement. However, the disadvantage of this procedure is that sometimes the reconstructed state is not physical [30].

Other method for finding parameters of the unknown state is using statistical treatment to solve the problem. The Maximum Likelihood (ML) method could be used for this purpose. The ML approach estimates the state and preserves fundamental properties of the reconstructed density matrix, particularly the positive semidefiniteness [30, 31]. The ML procedure reconstructs state that most likely gives measured data. The core of the procedure is to maximize the likelihood functional

$$\mathcal{L}(\rho) = \prod_i p_i^{n_i} = \prod_i \text{Tr} [\rho \Pi_i]^{n_i}, \quad (12)$$

where n_i is the the rate of detecting a particular outcome i , Π_i is positive-operator-valued measure (POVM) element and ρ is estimated density matrix of our unknown state. If the measurement consists of projections onto pure states Ψ_i , the POVM elements become equivalent to projectors onto these states:

$$\Pi_i = |\Psi_i\rangle \langle \Psi_i|. \quad (13)$$

By taking into account Eq. (13), the maximum likelihood functional could be rewrote as

$$\mathcal{L}(\rho) = \prod_i \langle \Psi_i | \rho | \Psi_i \rangle^{n_i}. \quad (14)$$

It represents probabilities of finding the state in given projection. Polarization state analysis using ML procedure is described in [32]. In this Thesis, the ML procedure is used to reconstruct polarization states.

1.4 Quantum process tomography

When studying quantum processes, or quantum channels, the information about arbitrary quantum state transformation by this channel is required. The quantum channels could be described by the completely positive map. The map \mathcal{E} takes input state, described by the density matrix ρ_{in} ($\text{Tr}[\rho_{\text{in}}] = 1$), and transforms it to the output state ρ_{out} .

$$\rho_{\text{IN}} \xrightarrow{\mathcal{E}} \rho_{\text{OUT}} = \mathcal{E} [\rho_{\text{IN}}]. \quad (15)$$

Since the map \mathcal{E} operates from a space of states to another space of states, the trace preserving condition is required.

$$\text{Tr} [\mathcal{E}(\rho)] = \text{Tr} [\rho]. \quad (16)$$

The map, usually called process matrix or Choi matrix, has shape $2^{2N} \times 2^{2N}$, where N is number of qubits. It characterizes the effect on the system, coherent evolutions, decohering interactions, and losses [33]. For quantum filters and general quantum channels, the condition (16) is replaced with inequality

$$\text{Tr} [\mathcal{E}(\rho)] \leq \text{Tr} [\rho]. \quad (17)$$

The aim of quantum process tomography is to characterize the quantum process by a sequence of measurements and find the completely positive map of the quantum channel [34–36].

Process matrices presented in this Thesis were found using the ML procedure. This approach searches for a process that most likely gives measured data. The scheme of ML procedure for quantum processes is presented in [37] and it is based on maximizing the likelihood function

$$\mathcal{L}[\mathcal{G}] = \prod_{i,j} \left[\text{Tr} \left(\Pi^{(ij)} \rho_{\text{out}}^{(j)} \right) \right]^{f_{ij}}, \quad (18)$$

where $\Pi^{(ij)}$ are POVM elements respective to the measurement of the output state $\rho_{\text{out}}^{(j)}$ and f_{ij} is relative frequency of corresponding measured data.

2 Nematic liquid crystal technology

In the field of common displays, present for example in digital watches, calculators, or, in a more complex way, in televisions or monitors, the most frequent technology is based on nematic liquid crystals.

Liquid crystal is a liquid phase of matter, where molecules have the orientation order similar to crystals, but their spatial order is similar to liquids [24, 38]. Molecules of the nematic liquid crystals form a thread-like structure [38] and maintain parallel orientation (see Fig. 2)[24, 38]. This molecular alignment causes that refractive index, electrical conductivity, etc. are different in the directions of long axis and short axis of the “cigar-shaped” molecule [38].

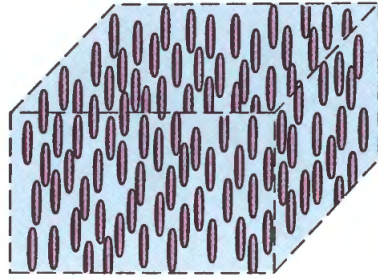


Figure 2: Parallel orientation of nematic liquid crystal (NLC) molecules [24].

The liquid crystal in a typical LC device is placed between two glass plates. These glass plates are on their inner sides covered by the electrodes made of a thin conducting layer of indium tin oxide (ITO), and by an organic layer with linear micro-grooves. The second mentioned layer is called alignment layer and molecules of liquid crystals tend to place themselves into the grooves [38]. This sets the primary orientation of molecules along the thickness of the device. If the orientation of two alignment layers is parallel, we talk about nematic liquid crystal (NLC) device. The other option is that the alignment layers on the front and back glass plates are oriented perpendicularly. Since the molecules of nematic liquid crystal tend to orient themselves parallel to each other, the typical helical structure is created [38, 39]. In this case, we talk about a twisted nematic liquid crystal (TN LC) device.

2.1 TN LC devices

The basic principle of a TN LC device operation is depicted in Fig. 3. In a state when a voltage is not applied on the device, the molecules of TN LC create helical structure. If linearly polarized light enters this module, the polarization of the light wave follows the helical structure of TN LC molecules (Fig. 3a). When one applies a voltage to the device, the molecules of the LC orient themselves along the electrical field. The light does not feel the birefringence property of the LC and thus, the polarization of the light is not changed (Fig. 3b)[39].

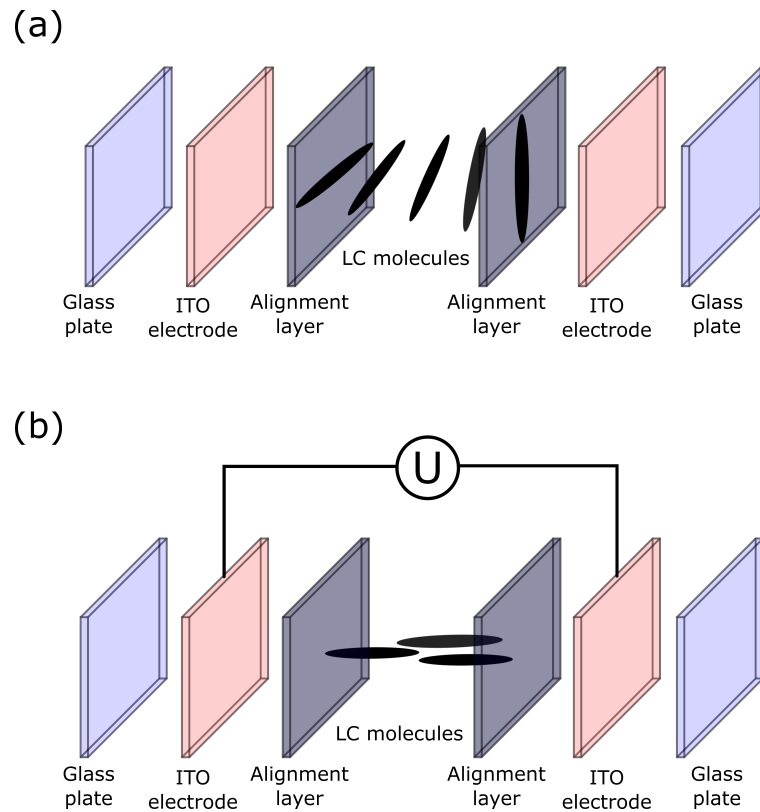


Figure 3: Basic structure and operational principle of a TN LC module. The module without applied voltage (a) and with applied voltage (b).

2.2 LC device drivers

Every LC module must be driven by a square wave signal with 0 V DC component. The DC component could damage the molecules causing malfunction of the device [40]. Any

voltage connected with LC module referenced further in the text is mentioned as peak-to-peak value. Drawing of typical square wave signal is shown in Fig. 4

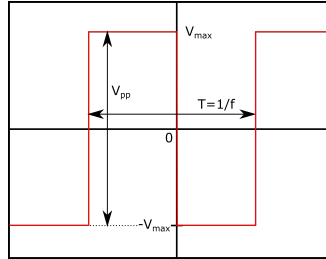


Figure 4: Driving voltage signal: V_{\max} - amplitude; V_{pp} - peak-to peak voltage; T - period; f - frequency.

For driving LC modules, custom drivers constructed by Mgr. Michal Dudka were used. These use microprocessor (μP) combined with analog switches or digital-analog converter (DAC) to generate the square signal for driving the LC modules. Two generations of this driver were constructed.

The first generation is based on synchronous polarity switching. The scheme of this generator is depicted in Fig. 5. When both switches are “up”, the positive voltage is applied on the upper electrode of the LC module. When switches flip to “down,” the polarity of signal applied on the module reverts. The switching of the two switches runs synchronously. Up to 8 LC modules can be operated with this driver, but one can not drive multiple segments with shared ground electrode due to polarity switching.

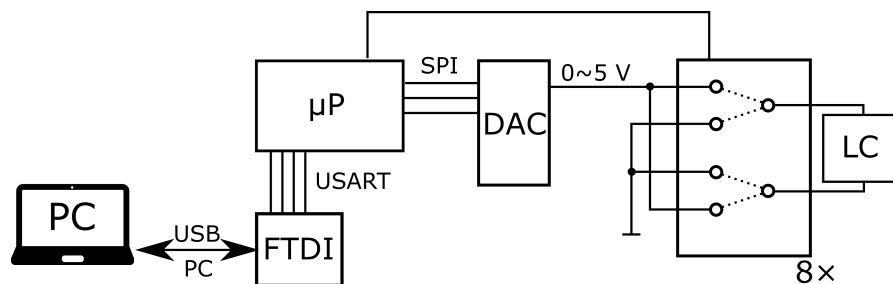


Figure 5: Schematic of the first generation of the LC driver constructed by Mgr. Michal Dudka.

Second, more advanced, generation of the device generates the square wave using fast DAC and amplifier. It also uses voltage reference for more precise voltage setting. Output

voltage is $V_{LC} = V_{DAC} - \frac{V_{ref}}{2} \cdot A$, where V_{DAC} is voltage on DAC, V_{ref} is reference voltage and A is a gain of the amplifier. Scheme of this generator is depicted in Fig. 6.

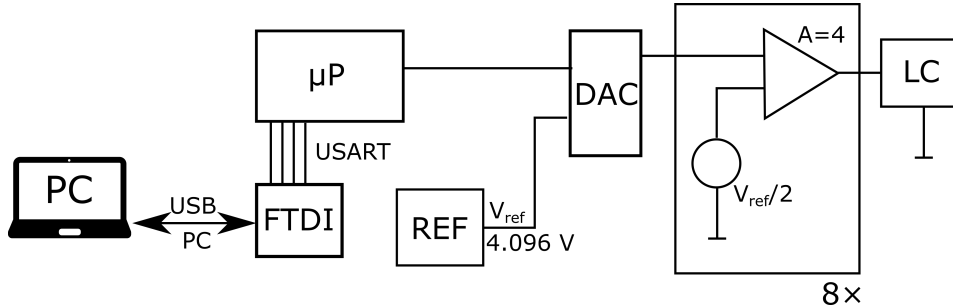


Figure 6: Schematic of the second generation of the LC driver constructed by Mgr. Michal Dudka.

2.3 Used LC modules

For purposes of experiments presented in this Thesis, LC modules based on standard TN LC displays were used. The TN LC module is made from the single-character TN LC display type LUMEX LCD-S101D14TR. The scheme and photo of this display is shown in Fig. 7. The TN LC module is created from this display by removing all outer polarization sheets, reflective layer, and protective layers (Fig. 8a). The bare glass module is then properly cleaned so all the remaining adhesive is removed. Such element is then ready to use in experiment. For easy manipulation with these modules, I have affixed each LC element to the rotation stage. This allows to rotate the TN LC module in plane perpendicular to direction of propagating light. The TN LC module in rotation stage is shown in Fig. 8b.

This particular type of LC module has voltage range $(0 - 10) V_{pp}$. Measurements were performed with frequency of driving signal $f = 1$ kHz ($T = 1$ ms). The transmissivity of this module was determined as $T = 0.86$. The bare LC module is not covered with any anti-reflective layer. Schematic figure of TN LC module, further used in this Thesis, is shown in Fig. 9.

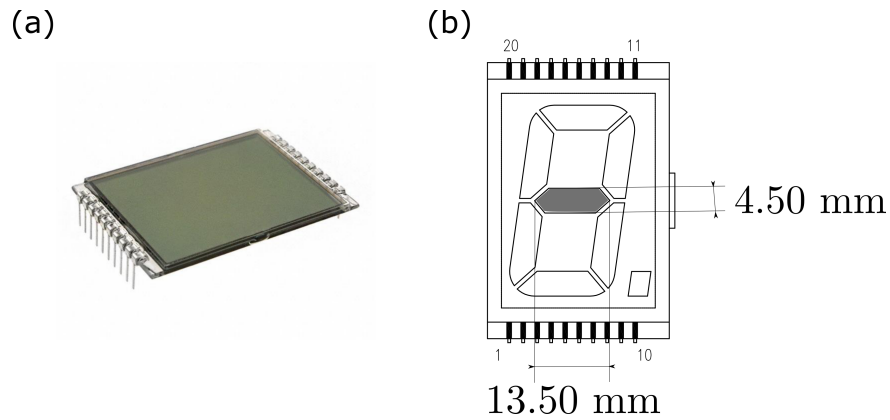


Figure 7: A photo of used TN LC display(a) and its scheme (b) with segment dimensions. Used segment is depicted as shaded region.

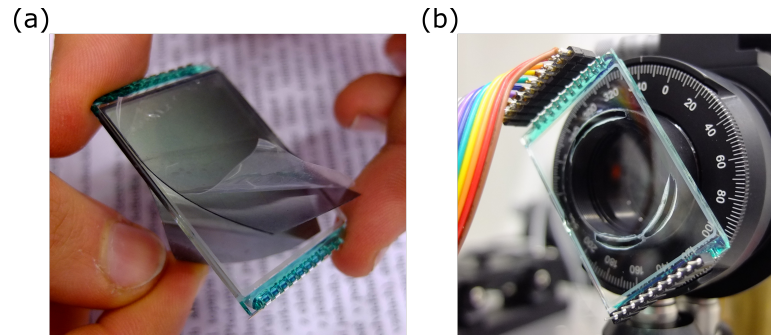


Figure 8: Photo of used TN LC display with partially removed polarization, reflection and protective layers (a) and photo of TN LC module in rotation stage placed in experimental setup (b).

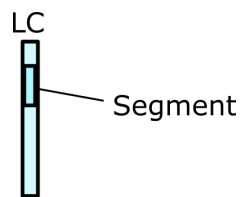


Figure 9: Schematic figure of TN LC module used in this Thesis. Segment means voltage-dependent area of the module.

3 Theoretical model

The Jones matrix of TN LC device could be derived using a sequence of infinitesimal polarization rotators and retarders [39, 41–43] and reads

$$J_{\text{TNLC}} = \begin{pmatrix} \cos \varphi & -\sin \varphi \\ \sin \varphi & \cos \varphi \end{pmatrix} \begin{pmatrix} \cos \chi - i \frac{\delta}{2\chi} \sin \chi & \frac{\varphi}{\chi} \sin \chi \\ -\frac{\varphi}{\chi} \sin \chi & \cos \chi + i \frac{\delta}{2\chi} \sin \chi \end{pmatrix}. \quad (19)$$

In this matrix, φ is a total twist angle and δ stands for difference of ordinary and extraordinary refractive index of the LC (retardance). Parameter χ relates retardation δ and twist angle φ by formula $\chi^2 = \varphi^2 + \left(\frac{\delta}{2}\right)^2$.

The retardance δ depends on a voltage applied to the LC module. Fig. 10 shows typical dependence of retardance on the applied voltage. These data were provided by ThorLabs company for their LC modules. As it is obvious from the graph, the dependence is strongly nonlinear. The image shows, that until certain voltage (“threshold” voltage), the retardance is constant. After passing the threshold voltage, the retardation rapidly decreases and for higher voltages it decreases slowly. Some authors describe this dependence with the arctan function [44]. However, the arctan function has symmetric shape. Thus, it cannot describe the asymmetry of the curve presented in Fig. 10. In this Thesis, the logistic function is used to model the dependence of retardance on applied voltage given by following formula:

$$\delta(V) = a + \frac{1}{b + \exp(d - cVe)}, \quad (20)$$

where V is voltage applied on the module and a, b, c, d and e are parameters.

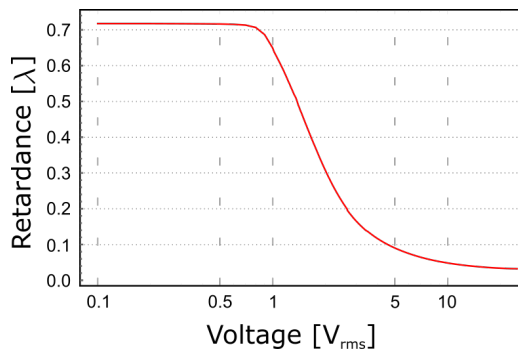


Figure 10: Dependence of retardance on applied voltage of LC device for laboratory use [45].

4 Single module characterization

If we want to work with TN LC modules, combine them in complex devices, and stack them into units, it is important to characterize the polarization transformation of a single module. For this purpose, the transformation of one TN LC module was measured.

The experimental setup is depicted in Fig. 11. The horizontally polarized light propagated through one segment of the LC module and the output polarization was measured. This measurement was performed for various voltages applied to the module. This experiment is described in depth in [46]. The whole procedure was repeated for a rotated LC module. During the experiment, the transformation was measured for 3 angles of rotation ($\alpha_1 = 0^\circ, \alpha_2 = 15^\circ, \alpha_3 = 30^\circ$). For each angle 200 voltages from interval $\langle 0, 10 \rangle$ V_{pp} were applied to the module. Results were fitted to the theoretical model consisting of matrix of the LC module (19) surrounded from both sides by a rotation matrix as

$$J_{\text{TOT}} = R(-\vartheta - \alpha_i) \cdot J_{\text{TNLC}} \cdot R(\vartheta + \alpha_i). \quad (21)$$

The additional rotation by angle ϑ was added to the model to determine the initial rotation angle and sign convention of the rotation. Angles $\alpha_i, i = \{1, 2, 3\}$ in Eq. (21) are known rotation angles. As the theoretical model of retardation $\delta(V)$ the Eq. (20) was used.

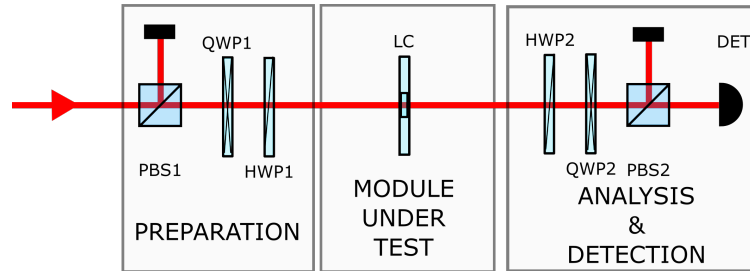


Figure 11: Scheme of experimental setup for characterization of LC module: polarization beamsplitter (PBS), quarter wave plate (QWP), half wave plate (HWP); LC module (LC), detection (DET). Detection part in this case consists of coupling into single mode optical fibre and decoupling in front of the PIN diode, where the signal is detected.

Results of this experiment are depicted in Fig. 12 as colour dots. Experimental data were fitted using the least squares procedure by searching for values of parameters mini-

mizing the following formula:

$$\sum_{l=\alpha_1, \alpha_2, \alpha_3} \sum_{m=1}^3 \sum_{n=1}^N (S_{m,n,l} - T_{m,n,l})^2. \quad (22)$$

Here $S_{m,n,l}$ is m^{th} Stokes parameter of measured output state when n^{th} voltage was applied to the module rotated by angle l . $T_{m,n,l}$ is the corresponding theoretical model for each $S_{m,n,l}$. Data for all three rotation angles were fitted at once. Fitted parameters are $\varphi = 65.8^\circ$, $\vartheta = 57.6^\circ$, $a = -9.34$, $b = 0.07$, $c = 188.51$, $d = -3.19$, $e = -2.94$. Fitted dependence of retardance on applied voltage is depicted in Fig. 13.

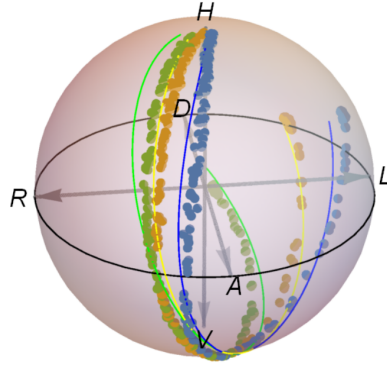


Figure 12: Transformation of a horizontally polarized light by a single TN LC module: rotation angle $\alpha_1 = 0^\circ$ (blue dots), rotation angle $\alpha_2 = 15^\circ$ (yellow dots), rotation angle $\alpha_3 = 30^\circ$ (green dots). Solid lines represent theoretical fit.

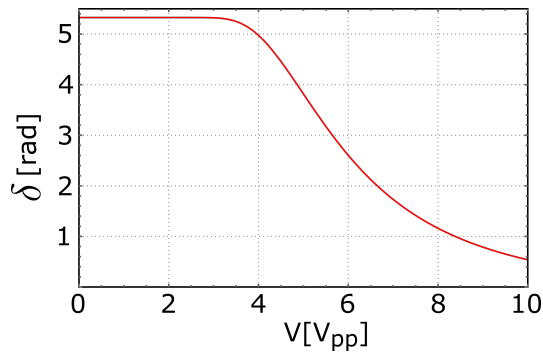


Figure 13: Dependence of retardance δ on voltage, fitted by the logistic function described by Eq. (20).

5 Polarization state preparation and analysis using LC modules

5.1 Minimal quantum state tomography

Many quantum information experiments based on photonic platform use polarization degree of freedom to encode the information. To gain the information, the polarization state has to be analysed. This could be performed in many ways. In our laboratory, the polarization state analysis is usually done by projecting the state onto six basis polarization states (H, V, D, A, R, and L). Projections are set using rotating quarter- and half-wave plates and a fixed polariser or polarizing beam splitter (PBS). The intensity of light or photon count rate is measured. This measurement represents relative frequency of finding the photon in projected state. These are used to estimate the polarization state. The estimation is done using the maximum-likelihood procedure described in Sec. 1.3.

To determine the polarization state of light, at least four projections need to be measured (see Sec. 1.3). The main idea of minimal quantum state tomography is to find four linearly independent states that decompose unit. Geometrically speaking, these four states create corners of an regular tetrahedron inscribed to the Poincare sphere with its corners on the surface of the sphere. These four POVM elements $\{\Pi_j\}$ create symmetric informationally complete POVM [47],

$$\sum_{j=1}^4 \Pi_j = 1. \quad (23)$$

The optimal regular tetrahedron, created by the four ideal states, takes maximal volume $V_{\text{opt}} = \frac{1}{6\sqrt{2}} \left(\sqrt{\frac{8}{3}}\right)^3$. This volume can be used as a measure of a quality of found tetrahedron.

For example *A. Ling et al.* in their experiments presented in [48] introduced the tetrahedron quantum state tomography without moving parts. The principle of their experiment was to prepare projections into four states using series of polarization beamsplitters and fixed wave plates. The advantage of this method is that required projections are measured simultaneously. On the other hand, this approach is applicable only for polarization state analysis and not for polarization state preparation. We can also prepare states creating optimal tetrahedron using TN LC modules. The experiment with one such element was performed by *A. Peinado et al.* in [49]. They used the LC module in various combinations with QWPs, linear polarisers, and mirrors to perform polarimetric measurements.

5.2 Wave plate preparation and analysis

First, the reference experimental setup was built with polarization state preparation and analysis using half- and quarter- wave plates. The scheme of experimental setup is depicted in Fig. 14. The main purpose to perform this experiment was to obtain data for later comparison of the traditional wave plate method and the proposed LC method.

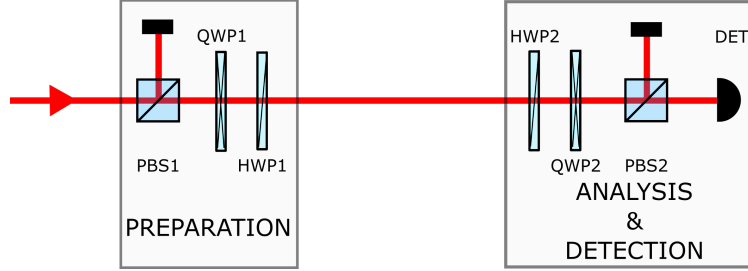


Figure 14: Scheme of experimental setup for polarization state preparation and analysis with polarization state preparation and analysis performed using rotating wave plates: polarization beamsplitter (PBS), half wave plate (HWP), quarter wave plate (QWP), detection (DET).

The beam was guided to the experiment from laser diode by single-mode optical fibre. The part of this fibre was mounted in polarization controller used for the total intensity adjustment. The light was then decoupled to free space by a collimator. The light propagated through the polarizing beam splitter PBS1 and the transmitted horizontal polarization was transformed by a series of quarter-wave plate QWP1 and half-wave plate HWP1. These wave plates prepared arbitrary polarization state. Afterwards, the polarization state was analysed with the half-wave plate HWP2, quarter-wave plate QWP2, and polarization beamsplitter PBS2. Finally, the light was coupled into a single-mode optical fibre and guided to the PIN diode detector. The experimental setup was built symmetrically, so the light could propagate in either direction and wave plates QWP2 and HWP2 can work as polarization state preparation.

The 6 states H, V, D, A, R, and L were prepared and reconstructed in this measurement and the process matrix of a free space was reconstructed using the maximum likelihood procedure. The reconstructed polarization states are shown in Tab. 1 and the reconstructed process matrix is depicted in Fig. 15. The reconstructed process has purity $P_{WP} = 1.000$ and fidelity $F_{WP} = 0.9986$ with the theoretical matrix of identity operation. The fidelity

was calculated using formula:

$$F = \frac{\text{Tr}[M_{\text{id}}M_{\text{ex}}]}{\text{Tr}[M_{\text{id}}] \text{Tr}[M_{\text{ex}}]}, \quad (24)$$

where M_{id} is idal matrix and M_{ex} is experimental matrix.

	H	V	D	A	R	L
S_1	-0.038	0.036	0.999	-0.997	-0.043	0.075
S_2	-0.031	0.033	0.041	-0.069	0.998	-0.997
S_3	0.999	-0.999	0.022	-0.034	0.056	0.027
DOP	1	1	1	1	1	1

Table 1: Reconstructed states: wave-plate preparation and analysis.

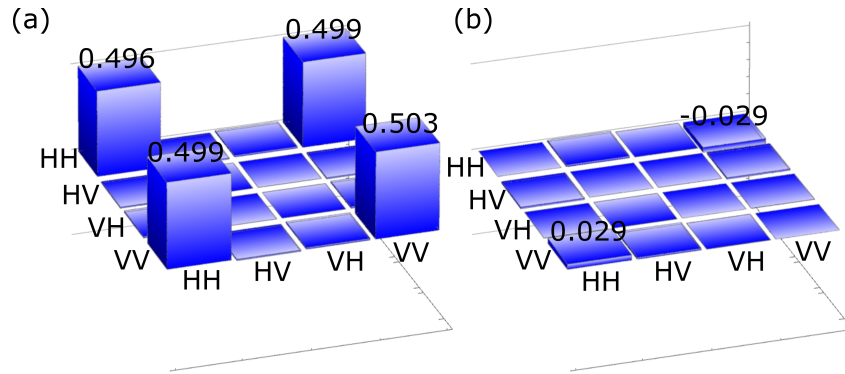


Figure 15: Reconstructed process matrix of free space: real (a) and imaginary (b) parts of the Choi matrix. States prepared and analysed with PBSs, HWPs and QWPs. Purity and fidelity of this process are $P_{\text{WP}} = 1.000$ and $F_{\text{WP}} = 0.9986$, respectively.

5.3 LC PA unit 1

After this measurement, the wave plates on polarization state preparation were replaced by the sequence of two LC modules assembled into the LC unit (LC PA unit 1). A photo and scheme of this unit is shown in Fig. 17. Scheme of the experimental setup is illustrated in Fig. 16. The optimal angles and voltages to obtain the optimal tetrahedron were found. These values are summarized in the Tab. 2.

Reconstructed polarization states creating corners of the tetrahedron are summarized in Tab. 3. The tetrahedron is shown on Poincare sphere depicted in Fig. 18. Volume of

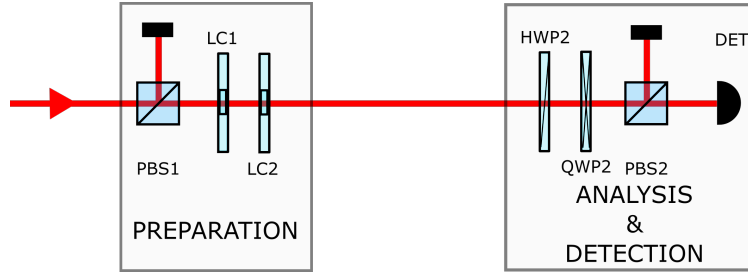


Figure 16: Scheme of the experimental setup for finding the optimal tetrahedron with the LC PA unit 1. The LC PA unit 1 prepared polarization states analysed with the wave plate analysis: polarization beamsplitter (PBS), half wave plate (HWP), quarter wave plate (QWP), detection (DET), LC module (LC).

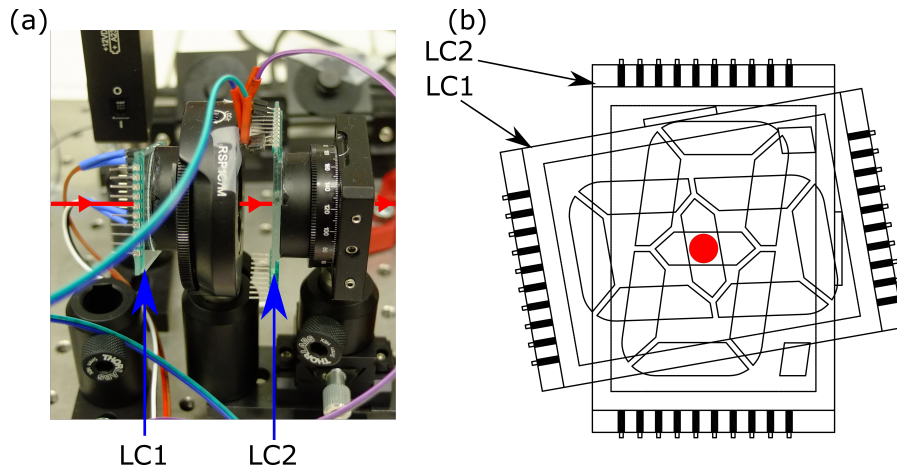


Figure 17: A photo of LC PA unit 1 (a). Red line represents propagating beam. Schema of LC PA unit 1 - front view (b). Red dot represents laser beam. It goes through an intersection of active segments of both LC modules.

the tetrahedron is $V_{\text{tet1}} = 0.998 V_{\text{opt}}$. Reconstructed density matrices of states Ψ_1 , Ψ_2 , Ψ_3 , and Ψ_4 were used as projectors in the maximum likelihood procedure and the experiment was reconfigured.

Next, the direction of light propagation was reversed. HWP2 and QWP2 now prepared the polarization state and LC PA unit 1 reconstructed the polarization state (scheme in Fig. 19). Results of 6 basis states (H, V, D, A, R and L) reconstruction are in Tab. 4. As we can see, the polarization state analysis using the LC PA unit 1 works well. If we compare the output states with ones achieved by conventional method of polarization analysis, we can see, that “LC-based” analysis gives even better results than the conventional method.

	ϑ	V_{Ψ_1}	V_{Ψ_2}	V_{Ψ_3}	V_{Ψ_4}
	[$^\circ$]	[V _{pp}]	[V _{pp}]	[V _{pp}]	[V _{pp}]
LC 1	85.5	8.18	8.54	5.42	3.75
LC 2	-33.0	6.85	4.75	4.54	9.91

Table 2: Orientation and voltages for reaching the optimal tetrahedron with LC PA unit 1.

	Ψ_1	Ψ_2	Ψ_3	Ψ_4
S_1	0.763	0.275	-0.827	-0.224
S_2	-0.223	-0.117	-0.530	0.965
S_3	0.606	-0.954	0.185	0.138
DOP	1	1	1	1

Table 3: Polarization states creating optimal tetrahedron prepared by LC PA unit 1 and reconstructed with wave plates.

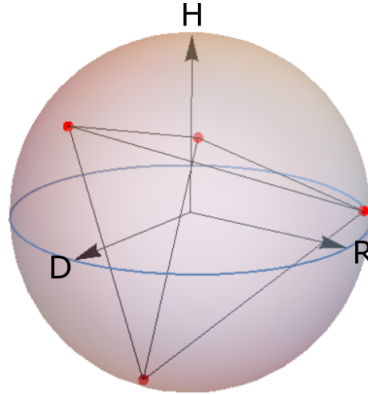


Figure 18: Polarization states (red dots) on Poincaré sphere creating optimal tetrahedron generated by LC PA unit 1.

5.4 LC PA unit 2

After the first LC unit was calibrated and tested in the experiment, the second one was constructed. For further applications, it was important to have a possibility to propagate two beams through one segment. Therefore, the second LC PA unit (LC PA unit 2) was

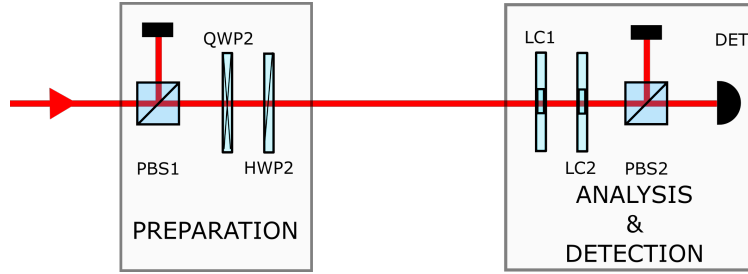


Figure 19: Scheme of experimental setup for polarization state preparation and analysis with wave plate preparation and analysis with LC PA unit 1: polarization beamsplitter (PBS), half waveplat (HWP), quarter wave plate (QWP), detection (DET), LC moule (LC).

	H	V	D	A	R	L
S_1	0.000	-0.011	1.000	-0.998	-0.042	-0.048
S_2	-0.042	-0.023	0.000	-0.065	0.998	-0.996
S_3	0.999	-1.000	0.023	-0.009	-0.043	-0.068
DOP	1	1	1	1	1	1

Table 4: Reconstructed states: wave-plate preparation and analysis using LC PA unit 1.

built using two parallel-oriented LC modules with horizontally aligned segments. The additional QWP oriented at 15° to its optical axis was placed between them. Photo and scheme of this unit is depicted in Fig. 20. The unit was characterized and optimal tetrahedron with volume $V_{\text{tet}2} = 0.993 V_{\text{opt}}$ was found. Voltages applied to LC modules in LC PA unit 2 to obtain the optimal tetrahedron are in Tab. 5. Tab. 6 shows Stokes parameters of states creating the optimal tetrahedron. This tetrahedron is also depicted on Poincare sphere in Fig. 21.

	V_{Ψ_1}	V_{Ψ_2}	V_{Ψ_3}	V_{Ψ_4}
	$[V_{\text{pp}}]$	$[V_{\text{pp}}]$	$[V_{\text{pp}}]$	$[V_{\text{pp}}]$
LC 3	6.01	4.03	3.85	9.21
LC 4	8.35	3.87	7.49	3.80

Table 5: Voltages for reaching the optimal tetrahedron with LC PA unit 2.

The combination of the two LC units was then used to perform reconstruction of process matrix of a free space. Scheme of this experimental setup is shown in Fig. 22. The

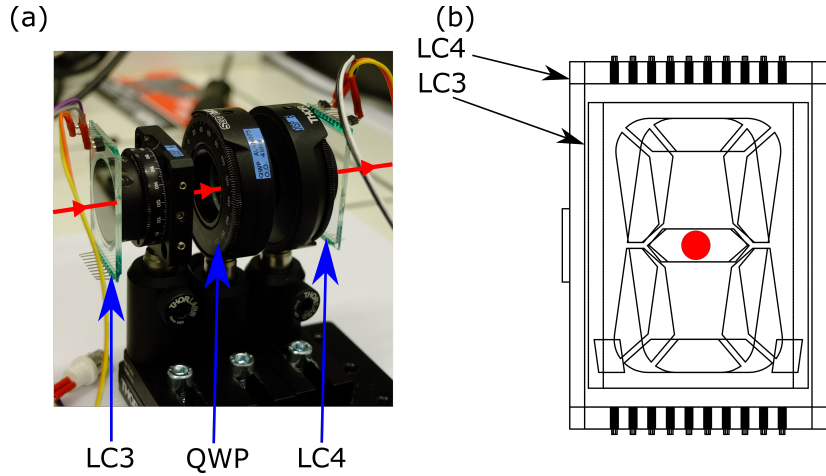


Figure 20: A photo of LC PA unit 2 (a). Red line represents propagating beam. Scheme of LC PA unit 2 - front view (b). Red dot represents propagating beam. It goes through an intersection of active segments of both LC modules.

	Ψ_1	Ψ_2	Ψ_3	Ψ_4
S_1	0.321	0.591	-0.953	0.072
S_2	-0.898	-0.323	0.031	0.654
S_3	-0.301	0.739	0.301	-0.753
DOP	1	1	1	1

Table 6: States creating optimal tetrahedron prepared by LC PA unit 2 and reconstructed by LC PA unit 1.

reconstructed matrix of the process is depicted in Fig. 23

As we can see, the reconstructed process matrix is in agreement with expected matrix. The “corner” elements of a real part of the matrix are well balanced and they differ from ideal value by 0.004 in the worst case. The imaginary part is non-zero but absolute values of all elements are below 0.02. The purity of the reconstructed process is $P_{LC} = 1.000$ and fidelity is $F_{LC} = 0.9993$.

We can compare results achieved by the conventional method, that is depicted in Fig. 15 and the result achieved with the polarization prepared and reconstructed using LC units depicted in Fig. 23. While purities of both matrices are the same, fidelities show that matrix achieved using the LC modules is slightly better ($F_{WP} = 0.9986$; $F_{LC} = 0.9993$).

The process matrix of a quarter wave plate oriented to its optical axis was also reconstructed using the two LC units as polarisation state preparation and analysis. The

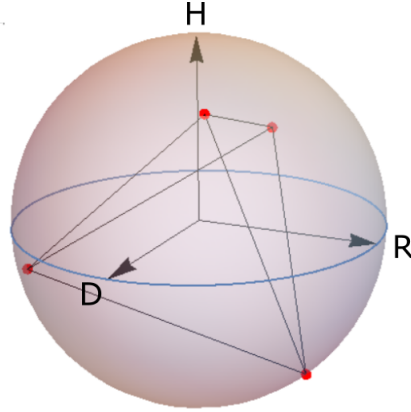


Figure 21: Polarization states (red dots) on Poincaré sphere creating optimal tetrahedron generated by LC PA unit 2.

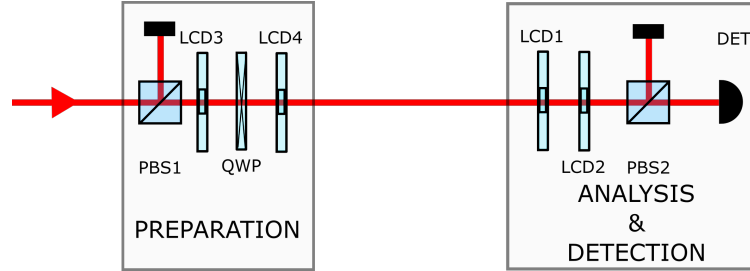


Figure 22: Scheme of experimental setup for polarization state preparation and analysis - LC preparation and analysis: polarization beamsplitter (PBS), quarter wave plate (QWP), detection (DET), LC module (LC).

quarter wave plate under test was placed between the polarisation state preparation and analysis, as shown in Fig. 24. The outcome process matrix of this measurement is depicted in Fig. 25. Purity of the process is $P_{\text{QWP}} = 1.000$ and process fidelity is $F_{\text{QWP}} = 0.995$. These values show that both the polarization state preparation and the analysis work well. The imbalance of the process matrix could be caused by imperfections of tested QWP.

5.5 The response of polarization preparation and analysis

One of the reasons to use LC modules for polarization state preparation and analysis is time spent by preparing the state. Conventional rotation of wave plates takes time in order of seconds to prepare one polarization state. If one wants to perform a conventional full process tomography of an N -qubit system, it requires 6^{2N} polarization state preparations consisting of a rotation of at least one wave plate. The time spent by wave plate movement

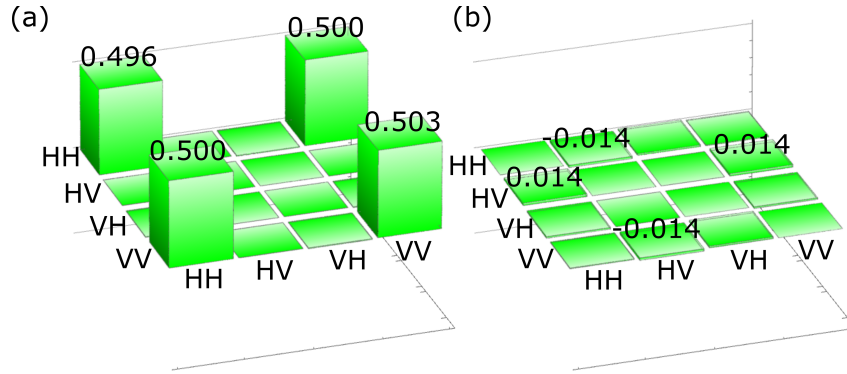


Figure 23: Reconstructed process matrix of free space: real (a) and imaginary (b) parts of the Choi matrix. The measurement was performed with LC unit 2 on state preparation and LC unit 1 on analysis. Purity and fidelity of this process are $P_{LC} = 1.000$. and $F_{LC} = 0.9993$, respectively.

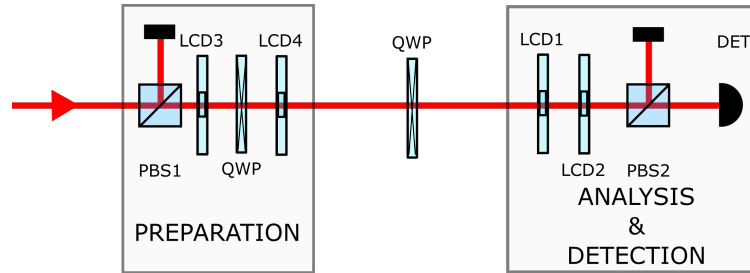


Figure 24: Scheme of experimental setup for measurement of process matrix of QWP using LC preparation and analysis: polarization beamsplitter (PBS), quarter wave plate (QWP), detection (DET), LC moule (LC).

then depends on a type of used rotation stages. Two types of motorized rotation stages are available in our laboratory, the “slow” rotation stage (Newport SR50CC), and the “fast” one (Newport PR50CC).

Every polarization state analysis requires at least one 45° rotation. The “fast” stage does this movement in approximately 5 s. For 6 reconstructed states, it is 30 s spent by this movement. Experiments presented in this chapter used both types of rotation stages. QWP1, HWP1, and HWP2 were placed in the “slow” motorized stage and QWP2 was placed in the “fast” stage. In this configuration, the time spent by wave plate movement during the measurement of a single polarization state was about 50 s. The total time spent by wave plate movement during process tomography was approximately 300 s. If one uses

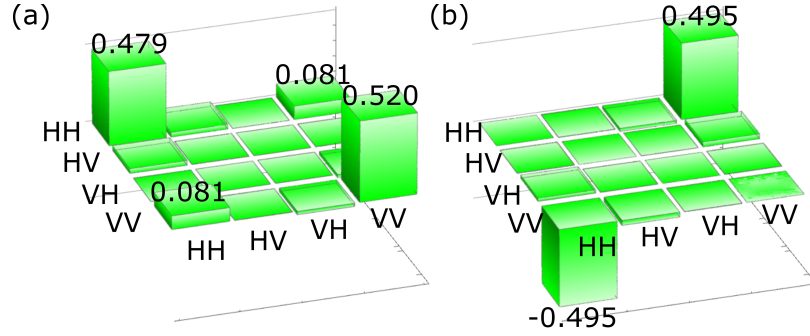


Figure 25: Reconstructed process matrix of a quarter wave plate oriented in its optical axis: real (a) and imaginary (b) parts of the Choi matrix. The measurement was performed with LC unit 2 on state preparation and LC unit 1 on analysis. Purity and fidelity of this process are $P_{\text{QWP}} = 1.000$ and $F_{\text{QWP}} = 0.995$, respectively.

minimal state tomography with all rotating wave plates in “fast” stages, the movement time would be at least 25 s.

On the other hand, LC units prepare or measure polarization states within time given by the response time of the LC module. The response time depends on many factors, such as temperature, thickness of the LC layer, and material properties of the LC (elastic constants, dielectric anisotropy etc.) [50–52]. The main reason for finite time response of LC on voltage changes is relaxation time of LC [51]. This time response is different for transitions from lower voltages to higher and for opposite voltage changes. The response is usually faster when going from lower voltages to voltages higher than half-wave voltage [53]. For that reason, the transition times of switching between two states were measured for TN LC unit 1, see Tab 7.

Final state \rightarrow	Ψ_1	Ψ_2	Ψ_3	Ψ_4
Initial state \downarrow				
Ψ_1	-	164	252	948
Ψ_2	146	-	216	952
Ψ_3	110	40.8	-	500
Ψ_4	126	190	238	-

Table 7: Measured transition times in ms when switching between two states of tetrahedron created by LC PA unit 1.

Using Tab. 7, we can determine the optimal sequence of the measurement to further shorten the time required for the polarization state tomography. In this case, the optimal sequence of measurements would be $\Psi_4 \rightarrow \Psi_3 \rightarrow \Psi_2 \rightarrow \Psi_1$ giving duration of $t \approx 425$ ms, which is approximately 2 times shorter than for the inverse sequence, used in previous measurements. However, the response time can be further compressed. There are several methods to shorten the response times. Most of the techniques are based on applying some other field to the LC. One approach uses magnetic field to shorten the response time [54]. However, the most methods for improving the response time uses the transient nematic effect [50, 51]. The basic idea is to apply maximal (“overshoot”) or minimal (“undershoot”) voltage for a short time before applying the required voltage [50, 53].

In a case of minimal process tomography, 4^{2N} measurements are performed. For 1 qubit, it is 16 measurements. Total time spent by measurement of one polarization state was approximately 4.2 s. Duration of process tomography, achieved in presented experiments, is about 17 s. This time includes polarization state preparations, reading the data from the multimeter, and time of the ML reconstruction procedure. Projection intensities were read out of the TTI 1906 multimeter. It is possible to read 3 to 4 data samples per second from this instrument. For each projection, 2 data samples were read out. The total time spent by data acquisition in process analysis was $16 \cdot 0.66 \doteq 10.6$ s. The residual time (≈ 2.6 s) was saved as a reserve. The time spent by polarization state preparation and analysis is comparable with the data acquisition time. However, if projections were measured in optimal order, the time for polarization state reconstruction would be reduced by roughly 2 s and duration of process reconstruction can be reduced by 5 s. The transient nematic effect can make the measurement even faster.

Let us consider the application of fast preparation and analysis of polarization encoded quantum bits carried by single photons. The new generation source of correlated single photons based on 6 mm thick periodically poled KTP nonlinear crystal yields $2.9 \cdot 10^6$ coincidences/s using 20 mW pump laser [55]. Usual setup, for example quantum logic gate e.g. Toffoli gate [56] or experiment for quantum state transfer [57], has transmissivity $\frac{1}{100}$ for coincidences. At the output, we obtain roughly $29 \cdot 10^3$ coincidences/s. For successful polarization state tomography, we typically need at least 100 coincidences in maximum. This gives minimal acquisition time of 3.4 ms. Because the average response time of the LC PA unit 1 in optimal configuration is about 170 ms, we can extend the data acquisition time. If we set data acquisition time to 100 ms, we can obtain about 2900 coincidences in maximum and thus, increase the precision of polarization state recon-

struction, while keeping the total time short.

In this chapter, I have shown that TN LC modules can be used for polarization state preparation and analysis. This technique, in comparison with the traditional method based on rotating wave plates, has several advantages. The first one is the speed of the measurement. The second advantage is that there is no physical movement of any element and all changes of polarization states are caused by voltage changes. Therefore, a precession of light beam due to imperfections (tilt or wedge) of the moving wave plates and, consequently, a modulation of optical fibre coupling efficiency, is removed.

Two configurations of LC PA units were constructed. The first LC PA unit was built with two TN LC modules. This unit is cheap, however, rotated configuration (see Fig. 17) means that it has to be adjusted in the experimental setup with high precision to avoid the beam passing partially out of the intersection of active segments. This kind of PA unit can be used only for one beam. The second LC PA unit uses configuration with horizontally oriented, parallelly aligned segments with QWP between LC modules. The main advantage of this configuration is that it is relatively simple to adjust it in the experiment because only vertical alignment of the two segments is crucial (see Fig. 20). It also enables propagating more beams through one segment, making this unit usable in applications, where two closely spaced beams are present.

6 Polarization filter

Polarization filters serve to selectively attenuate one polarization component of entering light. They could be found in many quantum optics experiments, e.g., orthogonalization of unknown states [58], quantum control phase gate [59], and in remote state preparation [60]. The polarization filter can find application also in optical attenuators [61] for amplitude modulation, and optical shutters [16] applicable e.g. for conditional activation of light-matter interaction in quantum memory experiments. This setup is also used for switching between two paths [17], applicable e.g. in quantum key distribution [62, 63]. *K. Fischer et. al.* built an single qubit depolarizing channel using fast polarization changes provided by LC modules placed in an polarization interferometer [64]. Many of referenced articles show construction of these devices with LC modules. Polarization filters are usually built using polarization Mach-Zehnder interferometer.

6.1 Polarization interferometer

Polarization interferometers are usually used in applications that require transcription between polarization and spatial encoding of information and in applications that require long term stability. These are reasons why inherently stable polarization Mach-Zehnder interferometers are constructed. The basic principle of the interferometer could be described as follows.

The incident beam enters the calcite polarization beam displacer. The horizontal polarization feels extraordinary refractive index n_e , while vertical polarization feels ordinary refractive index n_o . This birefringence causes the spatial separation of the two polarisation components of the incident light. The distance between the two paths is determined by the length of the calcite crystal. The two separated paths are then combined back together on the second beam displacer. To achieve this, the half-wave plate oriented at 45° in respect to its optical axis is present in the setup, changing the horizontal polarization into vertical and vice-versa. The two beams then interfere on following polariser. Phase in the interferometer can be changed by tilting the beam displacers.

The scheme of polarization Mach-Zehnder interferometer is depicted in Fig. 26. Calcite beam displacers used in following experiments separate H and V beams by 4 mm. Visibility of the interference is calculated as

$$VIS = \frac{I_{\max} - I_{\min}}{I_{\max} + I_{\min}}, \quad (25)$$



Figure 26: Scheme of the polarization Mach-Zehnder interferometer: beam displacer (BD), half wave plate (HWP), polarization state preparation (P), polarization state analysis (A). The separation between the two paths is 4 mm.

where I_{\max} and I_{\min} are intensities in maximum and minimum of interference fringe, respectively.

6.2 Polarization filter with one LC module

The polarization filter was built using the polarization Mach-Zehnder interferometer. The experimental setup is schematically depicted in Fig. 27.

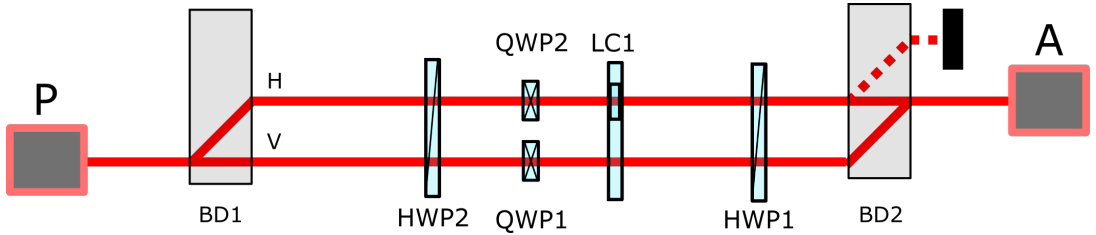


Figure 27: Scheme of polarization filter with one TN LC module: polarization state preparation (P), polarization state analysis (A), beam displacer (BD), half wave plate (HWP), quarter wave plate (QWP), liquid crystal module (LC).

One LC module was added to the Mach-Zehnder interferometer and arranged that one path of the interferometer was passing through the segment of the module, so its polarization state is changed with varying voltage. The second path passes through voltage independent area (off-segment). The filtration procedure than works as follows. The initial polarization (D) is spatially decomposed into H and V parts on the BD1. The H polarization in the upper arm of the interferometer is changed to D and in the lower arm from V to A by HWP2 rotated by 22.5° to its optical axis. Lower path then propagates through QWP1 and the off-segment area of the LC module (LC1). These together transform A polarization to D. The light in the lower path then propagates through HWP1 oriented

at 22.5° to its optical axis and rotates the polarization state from D to H. Light in the upper path after HWP2 propagates through segment of the LC module. The QWP2 before LC module preserves interference by compensating the path difference between upper and lower arm. Then it passes through HWP 1 and vertical part of the polarization is recollected with light propagated in lower arm. For maximal voltage applied to the LC module ($10 V_{pp}$), the polarization of upper path does not change and HWP1 rotates the D polarization to H and it is displaced by the BD2, causing that the light does not recollect with the lower path. If lower voltage is applied to the LC1, the amount of light from upper path merged with light from the lower path increases. When LC1 switches D to A, all the light from upper path is recollected and the output state is the same as input state. This experimental setup was evaluated by the means of full process tomography. To illustrate the action of the polarization filter, the filtration of D polarization state for various voltages applied to the LC module is depicted in Fig. 28.

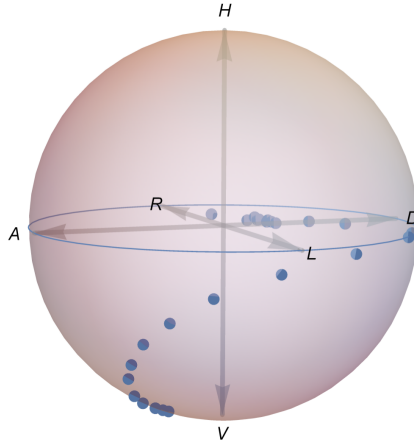


Figure 28: Polarization state (blue markers) at the output of the polarization filter as a function of applied voltage.

As we can see in Fig. 28, the polarization state detected at the output detector varies with voltage applied on the LC module. Until reaching certain voltage, the polarization state travels along the equator of the Poincaré sphere. This means, that for these voltages, only a phase is modulated with increasing voltage. After reaching the threshold voltage, the polarization filtration begins. With increasing voltage applied to the LC module, the H component of the input state is attenuated and the output polarization approaches the V state.

The advantage of this polarization filter realization is its simplicity. The filter uses the inherently stable Mach-Zehnder interferometer for transcription of information from polarization degree of freedom to spatial degree of freedom. The filtration itself is then performed by applying voltage on one LC module. However, the trajectory of the output polarization state does not follow the meridian of the Poincare sphere, but it moves along more complicated curve, where an additional phase shift has to be taken into account in possible applications.

The average visibility in this experiment was $(96.7 \pm 0.3)\%$ with a free space detector. It shows that even LC modules based on common LC displays with no advanced precision for laboratory use can be used in interferometric experimental setup and do not make drastic deformations of a wavefront.

In this section I have shown, that tunable filtration could be achieved with a simple LC module accompanied with two QWPs. Maximal filtration in this case is very high, however the polarization state transformation does not follow path along the meridian of the Poincare sphere. The additional phase shift is induced during the process of filtration. The advantage of this experimental setup is its simplicity, good stability, and speed of the state transformation.

7 Tunable phase modulator

Phase modulation is a useful tool in quantum optics and quantum information experiments. The phase change is a core of quantum CZ gate, which belongs to a set of basic quantum logic gates.

The tunable phase modulator with two LC modules was constructed using the polarization Mach-Zehnder interferometer. One path of the interferometer propagated through in-segment regions of the LC modules, while the second path passed through off-segment regions, as illustrated in the scheme of the experiment in Fig. 29.

Between the two LC modules a HWP oriented at 45° in respect to its optical axis is placed.

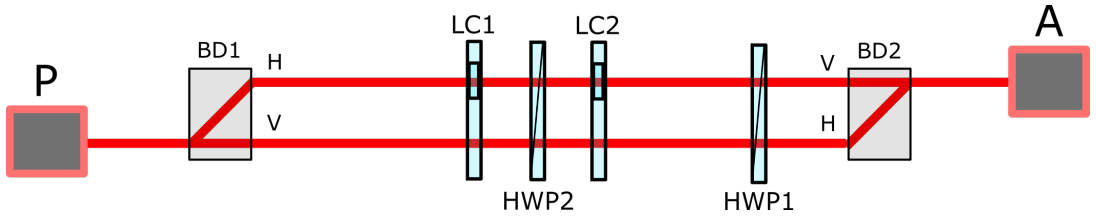


Figure 29: Scheme of polarization filter with 1 LC module: polarization state preparation (P), polarization state analysis (A), beam displacers (BD), half-wave plate (HWP), quarter wave plate (QWP), liquid crystal module (LC).

This causes, that while the lower path of the interferometer feels fixed phase change, the change of phase in the upper path of the interferometer depends on the voltages applied to the LC modules. Because the voltage dependences of LC1 and LC2 are shifted, voltage applied to LC1 satisfies $V_{LC1} = V_{LC2} - 0.17 V_{pp}$. Further in this chapter, the mentioned voltages will correspond to V_{LC2} . To illustrate the results of this experiment, the output polarization state is depicted in Fig. 30.

If phase between the horizontal and vertical polarization is changed, the polarization state measured at the output of the experiment (part “A” in Fig. 29) goes only along the equator of the Poincare sphere. If polarization state in one path changes, the balance between H and V would not be preserved and the experimental setup would work as polarization filter described in Sec. 6. Fig. 30 clearly shows that the output polarization state follows the equator of the Poincare sphere. The whole equator is not covered due to maximal retardance of the used module, that is smaller than 2π . Red dots in Fig. 30 represent 7 states on equator of Poincare sphere prepared by wave plates (the stage P in

Fig. 29). The average visibility during these measurements was 95%. This means, that visibility decreased by approximately 1.5% when second LC module was inserted into the interferometer.

This experimental setup could be used to prepare an arbitrary state on the equator of the Poincare sphere. For example one can prepare 4 of 6 basis states (D, A, R and L) and switch between them very fast. The following table (Tab. 8) shows voltages that correspond to particular states on the equator of the Poincare sphere with D polarization on input.

V_{LC2} [V _{pp}]	Output state
3.80	D
4.80	R
5.65	A
7.18	L

Table 8: Voltages applied to LC modules to prepare concrete states on the equator of the Poincare sphere.

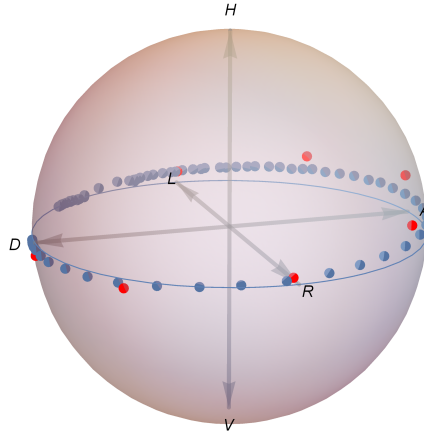


Figure 30: Output polarization states (blue dots) after propagating through a setup working as phase modulator. Solid blue circle represents the equator of the Poincare sphere. Red dots stand for polarization states prepared by rotating wave plates.

8 Polarization filter with phase modulator

It is usually good to perform filtration along meridian of the Poincare sphere because it does not add any phase shift. The filter presented in Sec. 6.2 does not provide such transformation, as the trajectory on the Poincare sphere is not simple. The “meridian” trajectory can be achieved by combining the simple filter setup presented in Sec. 6 and phase modulator, presented in Sec. 7.

The scheme of this setup is shown in Fig. 31. The light from laser diode is guided through a PM fibre to collimator where it is decoupled to the free space. Then the polarization state is prepared by propagating through a polariser and a sequence of HWP and QWP (part P in Fig. 31). When the polarization state is prepared, its H and V parts are spatially separated at the BD1. Then the light enters the phase-modulation part of the experiment. The necessary phase shift between the two beams for compensation of the non-trivial action of the simple filter is applied by setting proper voltage on LC modules 1 and 2 (LC1, LC2). The filtration part then works exactly the same as presented in Sec. 6. The process of finding the proper phase modulation for achieving the meridian

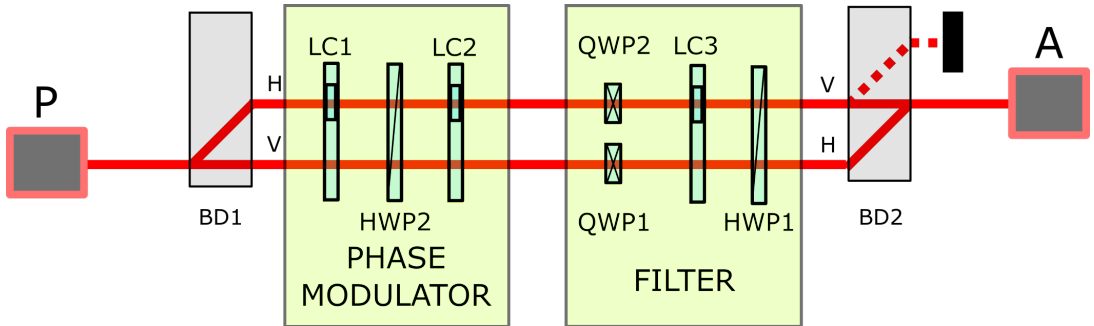


Figure 31: Scheme of the filter with combination with phase modulator: polarization state preparation (P), polarization state analysis (A), beam displacer (BD), half wave plate (HWP), quarter wave plate (QWP), liquid crystal modules (LC1, LC2, LC3).

trajectory was done as follows. Let us have polarization state $|\Psi\rangle$ located at the equator of the Poincare sphere. We want to apply filtration of this state along meridian that passes through this state. First, we set the proper voltage to the filtration LC module. Then the projection onto $|\Psi^\perp\rangle$ is set at analysis stage of the experiment (part A in Fig. 31). In the next step, the minimum intensity is found by varying voltages applied to the modulation part of the experiment. As we can see in Fig. 33, this method works better for states closer to the equator of the Poincare sphere. Closer to the pole of the Poincare sphere, the

projections onto state on the equator are closer to $\frac{I_{\max}}{2}$ and varies less with changing phase modulation. This causes that the false minimum could be found due to intensity fluctuations. Alternatively, the phase modulator can be calibrated and compensation phase shift can be set directly instead of finding the minimum signal at the orthogonal projection.

The visibility during this experiment was 99%. The improvement in comparison with the previous experiments is due to coupling into the single mode fibre, after propagating through polarization state analysis. This is a good result because the slight wavefront distortion caused by multiple LC modules could be removed.

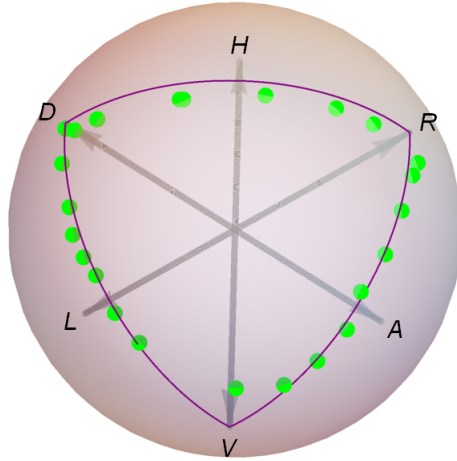


Figure 32: Various polarization states achieved using the combination of the phase modulator and the filter. Green dots represent measured data. Purple arcs represent parts of meridians (arcs going from D or R to V) and the equator (arc connecting D and R) of the Poincare sphere.

Fig. 33 shows that the output polarization state changes along the meridians of the Poincare sphere. We can choose, which meridian trajectory the polarization state follows by setting proper projection when finding minimum during the phase-compensation procedure. The filtration could be turned off and the experimental setup can work as phase modulator (part of the trajectory along the equator in Fig. 33).

The phase-compensated filter was created by combining the experimental implementations of phase modulator (Sec. 7) and simple filter (Sec. 6). Using this configuration, the

trajectory along the meridian was achieved by compensating phase shift induced during filtration. The filtration along any meridian of the Poincare sphere can be achieved simply by applying proper voltages onto the phase modulator. The big advantage of this experimental realization of polarization filter is its simple application in experiments that work with polarization filters. During implementation of this method, only calibration consisting of finding proper voltages for modulation and filtration need to be found. Another advantage is the speed, given by the response time of the LC modules.

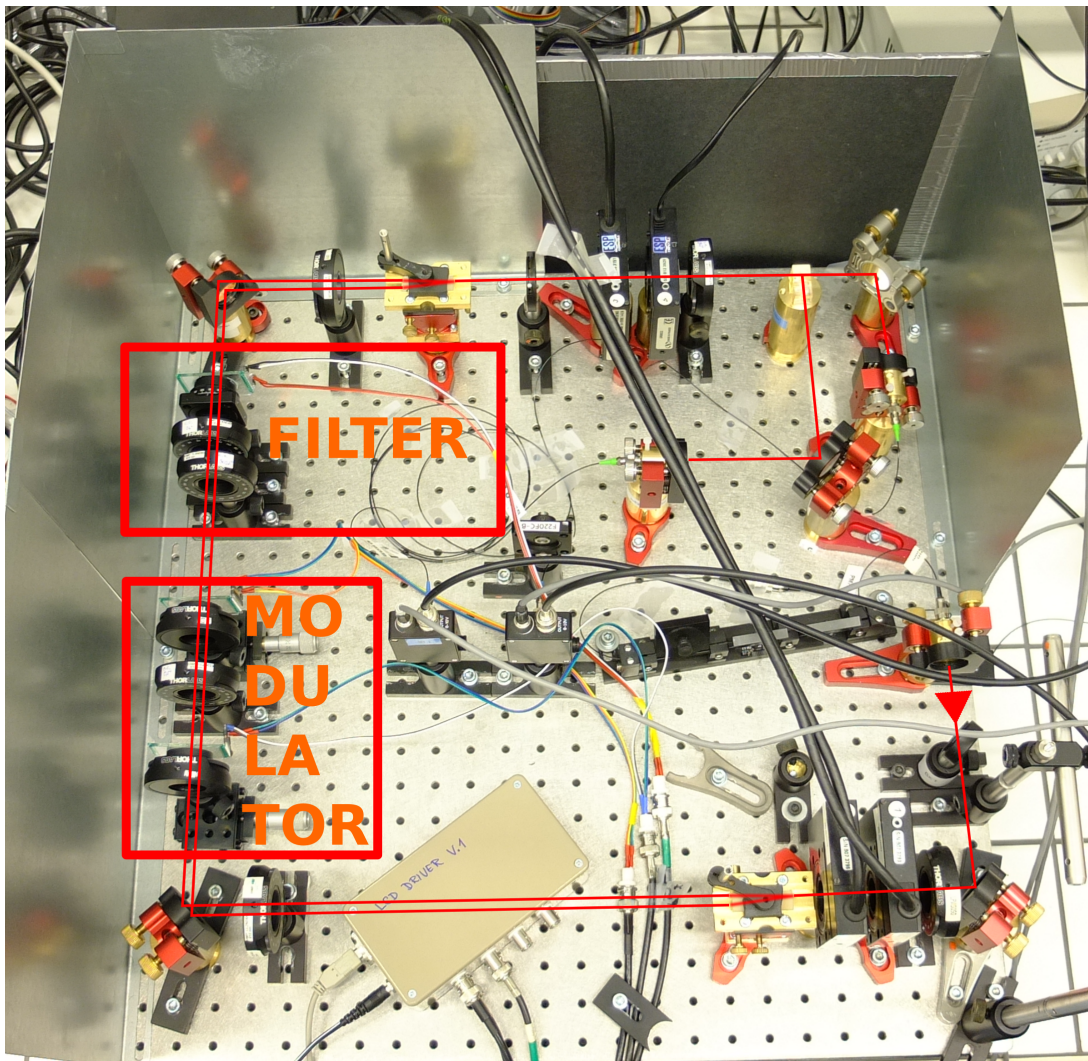


Figure 33: A photo of the experimental setup with 3 LC modules creating polarization filter and phase modulator. The red line represents propagating beam.

Conclusion

In this Thesis, I have worked with twisted nematic liquid crystal devices, based on LC displays commonly used in consumer electronic devices, such as calculators, digital watches etc. Results of my experiments show that even this kind of modules can find use in quantum optics experiments. They can find applications in polarization filters and phase modulators. Great application of these elements is in polarization state preparation and analysis, where they can replace standard quarter and half waveplates. The LC based devices provide us faster measurements with the same or better output qualities as conventional methods.

Polarization state preparation performed in Sec. 5 used LC PA units to perform the minimal qubit state tomography. Two LC PA units were assembled. The first unit contains two LC modules. By applying proper voltages, optimal tetrahedron for minimal quantum state tomography, with volume $V_{\text{tet1}} = 0.998 V_{\text{opt}}$, has been found. This unit has been used to perform the tomography of polarization states. Later, second unit (LC PA unit 2) has been assembled containing two LC modules and a quarter wave plate. Its photo and scheme are depicted in Fig. 20. The optimal tetrahedron created by this unit has been found and in combination with LC PA unit 1, it was used to perform the process reconstruction. The reconstructed matrix of a process of a free space reaches fidelity $F = 0.9993$. All the results show that polarization state preparation and analysis using LC modules work well and parameters describing the quality of measurements, such as fidelity and purity, are the same or slightly better than ones obtained by conventional methods. Using the LC units the total time of tomography of process ≈ 17 s has been achieved. The effect of the response time of LC modules on measurement duration has been discussed and further steps for optimization of the measurement time have been proposed. These consist of optimization of measurement ordering and more complex methods of driving LC modules.

Experiments presented in Sec. 6, Sec. 7, and Sec. 8 use LC modules in inherently stable polarization Mach-Zehnder interferometer. In different experiments, up to three LC modules were present in the experimental setup. The visibility of the interferometer decreased by approximately 1.5% with each LC module added. The almost perfect visibility of 99% has been restored when the output was coupled into single mode optical fibre.

Polarization filter in inherently stable Mach-Zehnder interferometer has been presented

in Sec. 6. The filtration is determined by voltage applied on the LC module. The result of this experiment shows that this configuration adds a phase shift to the output polarization state and the trajectory on the Poincare sphere is not simple. This kind of filter can find applications in amplitude modulators, however, faster methods such as Pockels cells would be more suitable for this purpose. In applications, such as arbitrary state orthogonalization or qubit transfer, the additional phase shift would have to be taken into account.

The tunable phase modulator has been introduced in Sec. 7. It works in polarization Mach-Zehnder interferometer and the phase shift between horizontal and vertical polarization has been realised using two LC modules. The trajectory of the output state on the Poincare sphere follows the equator. This shows that only phase between H and V polarization is changed.

Last experiment, presented in Sec. 8 of this Thesis, combines the phase modulator presented in Sec. 7 and the filter presented in Sec. 6. The combination of the two devices works as polarization filter, which does not add any phase shift. Using this experimental setup, we can perform filtration, phase modulation or both operations at once. This gives us universal tool for preparing any polarization state on one hemisphere of the Poincare sphere, starting from an arbitrary state laying at the equator. This experiment contains three LC modules and the quality of the output states (purity) is preserved. This shows the scalability of the LC approach.

Experiments presented in this Thesis can find applications in a broad spectrum of quantum information experiments. Every quantum gate working with qubits encoded into polarization degree of light can use TN LC units for polarization state preparation and analysis. The time consumption of either polarization state preparation and analysis could be reduced by factor of a 10 relative to currently used standard methods. This opens the possibility to perform experiments that require very long time, thus, can not be performed at the moment. Units presented in this Thesis will be used for measuring entanglement of two photons generated by the recently constructed source of entangled photons.

Phase modulators using LC modules, as presented in this Thesis, can be used in experiments dealing with adaptive quantum state discrimination, where they can switch measurement basis on the equator of polarization state in a real time by including proper feed-back.

References

- [1] J. L. O'Brien, *Science* **318**, 1567 (2007).
- [2] H. Häffner, C. Roos, and R. Blatt, *Phys. Rep.* **469**, 155 (2008).
- [3] J. Clarke and F. K. Wilhelm, *Nature* **453**, 1031 (2008).
- [4] P. Kok, W. J. Munro, K. Nemoto, T. C. Ralph, J. P. Dowling, and G. J. Milburn, *Rev. Mod. Phys.* **79**, 135 (2007).
- [5] D. P. DiVincenzo, *Fortschr. Phys.* **48**, 771 (2000).
- [6] E. Knill, R. Laflamme, and G. J. Milburn, *Nature* **409**, 46 (2001).
- [7] H. Takesue, S. D. Dyer, M. J. Stevens, V. Verma, R. P. Mirin, and S. W. Nam, *Optica* **2**, 832 (2015).
- [8] J. Yin, J.-G. Ren, H. Lu, Y. Cao, H.-L. Yong, Y.-P. Wu, C. Liu, S.-K. Liao, F. Zhou, Y. Jiang, X.-D. Cai, P. Xu, G.-S. Pan, J.-J. Jia, Y.-M. Huang, H. Yin, J.-Y. Wang, Y.-A. Chen, C.-Z. Peng, and J.-W. Pan, *Nature* **488**, 185 (2012).
- [9] B. Hensen, H. Bernien, A. E. Dreau, A. Reiserer, N. Kalb, M. S. Blok, J. Ruitenbergh, R. F. L. Vermeulen, R. N. Schouten, C. Abellan, W. Amaya, V. Pruneri, M. W. Mitchell, M. Markham, D. J. Twitchen, D. Elkouss, S. Wehner, T. H. Taminiiau, and R. Hanson, *Nature* **526**, 682 (2015).
- [10] K. Hirabayashi, *Appl. Opt.* **44**, 3552 (2005).
- [11] I. Moreno, J. L. Martínez, and J. A. Davis, *Appl. Opt.* **46**, 881 (2007).
- [12] Z. Zhuang, S.-W. Suh, and J. S. Patel, *Opt. Lett.* **24**, 694 (1999).
- [13] L. Dupont, J. L. Tocnaye, M. Gadonna, and T. Sansoni, *Ann.Télécommun.* **58**, 1364.
- [14] A. Orioux, L. Sansoni, M. Persechino, P. Mataloni, M. Rossi, and C. Macchiavello, *Phys. Rev. Lett.* **111**, 220501 (2013).
- [15] D. S. Naik, C. G. Peterson, A. G. White, A. J. Berglund, and P. G. Kwiat, *Phys. Rev. Lett.* **84**, 4733 (2000).
- [16] N. Spagnolo, C. Vitelli, S. Giacomini, F. Sciarrino, and F. D. Martini, *Opt. Express* **16**, 17609 (2008).

- [17] N. A. Riza, *Opt. Lett.* **19**, 1780 (1994).
- [18] J. Kempe, *Contemp. Phys.* **44**, 307 (2003).
- [19] A. M. Childs, *Phys. Rev. Lett.* **102**, 180501 (2009).
- [20] Y.-y. Zhao, N.-k. Yu, P. Kurzyński, G.-y. Xiang, C.-F. Li, and G.-C. Guo, *Phys. Rev. A* **91**, 042101 (2015).
- [21] M. Baranek, P. Bouchal, and Z. Bouchal, in *Digital Holography & 3-D Imaging Meeting* (Optical Society of America, 2015) p. DW2A.12.
- [22] C. Kohler, X. Schwab, and W. Osten, *Appl. Opt.* **45**, 960 (2006).
- [23] J. Běhal, *Charakteristika činnosti prostorového modulátoru světla*, Diploma thesis, Univerzita Palackého v Olomouci, Přírodovědecká fakulta, Olomouc (2015).
- [24] B. E. A. Saleh and M. C. Teich, *Fundamentals of photonics* (John Wiley & Sons, 1991).
- [25] D. Goldstein, *Polarized Light* (CRC Press, 2003).
- [26] R. C. Jones, *J. Opt. Soc. Am.* **31**, 488 (1941).
- [27] P. Kok and B. W. Lovett, *Introduction to Optical Quantum Information Processing*, Vol. 1 (Cambridge University Press, 2010).
- [28] D. F. V. James, P. G. Kwiat, W. J. Munro, and A. G. White, *Phys. Rev. A* **64**, 052312 (2001).
- [29] J. Altepeter, E. Jeffrey, and P. Kwiat, “Photonic state tomography,” in *Advances In Atomic, Molecular, and Optical Physics*, Vol. 52, edited by P. Berman and C. Lin (Academic Press, 2005) pp. 105 – 159.
- [30] M. Ježek, J. Fiurášek, and Z. Hradil, *Phys. Rev. A* **68**, 012305 (2003).
- [31] Z. Hradil, *Phys. Rev. A* **55**, R1561 (1997).
- [32] Z. Hradil, J. Řeháček, J. Fiurášek, and M. Ježek, “Maximum-likelihood methods in quantum mechanics,” in *Quantum State Estimation*, edited by M. Paris and J. Řeháček (Springer Berlin Heidelberg, Berlin, Heidelberg, 2004) pp. 59–112.

- [33] M. W. Mitchell, C. W. Ellenor, S. Schneider, and A. M. Steinberg, *Phys. Rev. Lett.* **91**, 120402 (2003).
- [34] J. L. O'Brien, G. J. Pryde, A. Gilchrist, D. F. V. James, N. K. Langford, T. C. Ralph, and A. G. White, *Phys. Rev. Lett.* **93**, 080502 (2004).
- [35] J. F. Poyatos, J. I. Cirac, and P. Zoller, *Phys. Rev. Lett.* **78**, 390 (1997).
- [36] I. L. Chuang and M. A. Nielsen, *J. Mod. Opt.* **44**, 2455 (1997).
- [37] J. Fiurášek and Z. Hradil, *Phys. Rev. A* **63**, 020101 (2001).
- [38] H. Kawamoto, *Proceedings of the IEEE* **90**, 460 (2002).
- [39] D.-K. Yang and S.-T. Wu, "Optical modeling methods," in *Fundamentals of Liquid Crystal Devices* (John Wiley & Sons, 2014) pp. 87–125.
- [40] S. H. Perlmutter, D. Doroski, and G. Moddel, *Appl. Phys. Lett.* **69** (1996).
- [41] A. Yariv and P. Yeh, *Optical waves in crystal propagation and control of laser radiation* (John Wiley & Sons, 1983).
- [42] P. Yeh and C. Gu, *Optics of liquid crystal displays*, Vol. 67 (John Wiley & Sons, 2010).
- [43] D.-K. Yang, *Fundamentals of liquid crystal devices* (John Wiley & Sons, 2014).
- [44] A. Vargas, R. Donoso, M. Ramírez, J. Carrión, M. Sánchez-López, and I. Moreno, *Optical Review* **20**, 378 (2013).
- [45] ThorLabs, "LCC Retarders Performance Data," (2006).
- [46] V. Krčmarský, *Polarization state control using liquid crystals*, Bachelor thesis, Palacky University Olomouc, Faculty of Science, Olomouc (2014).
- [47] J. Řeháček, B.-G. Englert, and D. Kaszlikowski, *Phys. Rev. A* **70**, 052321 (2004).
- [48] A. Ling, K. P. Soh, A. Lamas-Linares, and C. Kurtsiefer, *Phys. Rev. A* **74**, 022309 (2006).
- [49] A. Peinado, A. Lizana, J. Vidal, C. Iemmi, and J. Campos, *Appl. Opt.* **50**, 5437 (2011).
- [50] S. Wu and C. Wu, *J. Appl. Phys.* **65** (1989).

- [51] I.-C. Khoo and S.-T. Wu, *Optics and nonlinear optics of liquid crystals*, Vol. 1 (World Scientific, 1993).
- [52] R. I. McCartney, in *SID Symposium Digest of Technical Papers*, Vol. 34 (Wiley Online Library, 2003) pp. 1350–1353.
- [53] Meadowlark Optics, Inc, “Response time in liquid-crystal variable retarders,” <http://www.meadowlark.com/store/applicationNotes/Response%20Time%20in%20Liquid%20Crystal%20Variable%20Retarders.pdf>, Meadowlark Optics material; Accessed: 2016-04-22.
- [54] B. Wang, X. Wang, and P. J. Bos, *J. Appl. Phys.* **96** (2004).
- [55] I. Straka, (2016), personal communication.
- [56] M. Mičuda, M. Miková, I. Straka, M. Sedlák, M. Dušek, M. Ježek, and J. Fiurášek, *Phys. Rev. A* **92**, 032312 (2015).
- [57] M. Miková, I. Straka, V. Krčmarský, M. Dušek, M. Ježek, J. Fiurášek, and R. Filip, “Faithful quantum state transfer between weakly coupled qubits,” (2016), submitted for publishing.
- [58] M. Ježek, M. Mičuda, I. Straka, M. Miková, M. Dušek, and J. Fiurášek, *Phys. Rev. A* **89**, 042316 (2014).
- [59] K. Lemr, A. Černoč, J. Soubusta, K. Kieling, J. Eisert, and M. Dušek, *Phys. Rev. Lett.* **106**, 013602 (2011).
- [60] N. A. Peters, J. T. Barreiro, M. E. Goggin, T.-C. Wei, and P. G. Kwiat, *Phys. Rev. Lett.* **94**, 150502 (2005).
- [61] G. Zhu, B. yan Wei, L. yu Shi, X. wen Lin, W. Hu, Z. di Huang, and Y. qing Lu, *Opt. Express* **21**, 5332 (2013).
- [62] I. Marcikic, H. de Riedmatten, W. Tittel, H. Zbinden, and N. Gisin, *Nature* **421**, 509 (2003).
- [63] P. A. Hiskett, D. Rosenberg, C. G. Peterson, R. J. Hughes, S. Nam, A. E. Lita, A. J. Miller, and J. E. Nordholt, *New J. Phys.* **8**, 193 (2006).
- [64] K. A. G. Fisher, R. Prevedel, R. Kaltenbaek, and K. J. Resch, *New J. Phys.* **14**, 033016 (2012).